Computational Insight into ^{103}Rh Chemical Shift–Structure Correlations in Rhodium Bis(Phosphine) Complexes

Manuel A. Ortuño,[§] *Ludovic Castro*[‡] *and Michael Bühl**[‡]

[§]Unitat de Química Física, Departament de Química, Universitat Autònoma de Barcelona, 08193 Cerdanyola del Vallès, Barcelona, Spain.

[‡]School of Chemistry, University of St Andrews, North Haugh, St Andrews, Fife KY10 9ST, UK.

*Corresponding author: mb105@st-andrews.ac.uk

Abstract

^{103}Rh NMR chemical shifts have been computed at the GIAO-B3LYP level of density functional theory (DFT) for a number of $[Rh(COD)(P\cap P)]^+$ complexes [COD = 1,5-cyclooctadiene, P∩P = chelating bis(phosphine) including bis(dimethylphosphino)ethane (dmpe), bis(diphenylphosphino)ethane (dppe), MeDUPHOS, DIOP, BINAP and others]. Structures have been optimized using PBE0 and M06 functionals in the gas phase, in a continuum modeling the solvent, and with $[PF_6]^-$ counteranion included explicitly. Observed trends in $\delta(^{103}Rh)$ are well reproduced for pristine PBE0-optimized cations in the gas phase, or for ion pairs optimized in a continuum with M06. While there is no overall trend between computed $\delta(^{103}Rh)$ values and complex stabilities (evaluated through isodesmic ligand exchange reactions), there is a linear relationship between the ^{103}Rh chemical shifts and the mean Rh–P bond distances. This relationship appears to be remarkably general, encompassing various chelating ring sizes and substituents at P, including remote electron-donating and -withdrawing substituents that are characterized through their Hammett constants. The combination of ^{103}Rh NMR and DFT computations emerges as useful tool for structure elucidation of Rh–phosphine complexes.

Introduction

Rhodium chemistry is a cornerstone in homogeneous catalysis since the corresponding complexes are key species in relevant processes such as hydrogenation reactions and hydroformylation of alkenes. The design of new and improved catalysts requires thorough analysis of such species. In order to obtain further insight, ^{103}Rh nuclear magnetic resonance (NMR) spectroscopy emerges as a captivating analytical tool to study the very center of these metal compounds,[1,2] including those of active catalysts.[3]

As rhodium complexes bearing phosphine ligands are particularly well suited to be studied with ^{103}Rh NMR spectroscopy, a wealth of experimental data is available.[2b–c,4,5,6] A priori there is no straightforward general relationship between chemical shifts and reactivity. However, a number of such relationships have been established empirically within closely related families of compounds.[2a] For instance, ^{103}Rh chemical shifts have been correlated with rate constants of ligand exchange[7] and migration reactions,[8] enantioselectivities,[9] and stability constants.[10] More recently, rates of water substitution processes in rhodium clusters have been shown to correlate with chemical shifts.[11] Similar NMR–reactivity relations have also been observed or predicted in other organometallic systems, e.g. using ^{59}Co[12] or ^{51}V NMR.[13] As a whole, transition metal NMR is a useful tool to study structural features as well as reactivities.

The chemical environment about the metal can be adjusted by tuning and tailoring the ligands. Quantum-chemical computations can be a valuable complement because they can be used to study ligands or ligand configurations that are not accessible experimentally, and to investigate properties of transition metal complexes in a systematic way. Theory can predict structures, energies, and NMR properties, and the resulting trends may be rationalized. In this regard, computational techniques based on density functional theory (DFT) have been successfully applied to reproduce ^{103}Rh chemical shifts, among other transition metals.[14,15] First computational studies on ^{103}Rh nuclei were devoted to organometallic compounds which span a sizeable chemical shift range of ca. 3600 ppm.[16,17] The scope of this methodology has been extended to species containing phosphines,[18,19] N-donor,[20] and alkene ligands,[21] as well as imidazole-based radiosensitizers.[22] Other complexes including indacenyl[23] and porphyrin[24] derivatives have also been analyzed.

The Rh–bis(phosphine) fragment has provided excellent results in catalytic processes such as hydrogenation reactions.[25] In this context, a series of cationic $[(COD)Rh(P\cap P)]^+$ complexes **1**–**7** (Figure 1, COD = 1,5-cyclooctadiene, P∩P = chelating bis(phosphine)), useful in hydrogenation of enamides,[26] has been studied recently, and their observed ^{103}Rh chemical shifts have been correlated with computed relative stabilities.[27] We now report geometries and ^{103}Rh chemical shifts of **1**–**7**, calculated with different and improved methodologies, allowing to select the most suitable one by direct comparison with experimental data. This methodology is then applied to a new extended set of compounds in which the steric and electronic properties of the ligands have

been varied systematically. The resulting chemical shift trends are analyzed with respect to several factors, i.e. ligand binding energies, bond distances, and Hammett constants, affording new insights into the interdependencies of these properties.

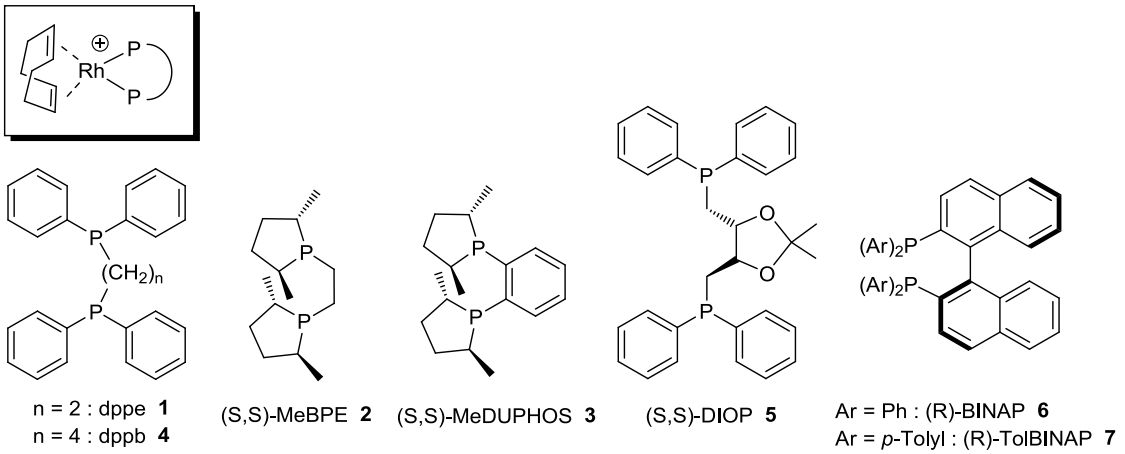

Figure 1. Rh–bis(phosphine) complexes **1**–**7** under study.

Computational Details

Geometries have been fully optimized at the DFT level using M06[28] (with an ultrafine grid)[29] and PBE0[30] functionals as implemented in Gaussian 09.[31] The M06 method accounts for dispersion interactions[32] whereas the PBE0 approach performs well to describe geometries of second row transition metal complexes.[33] Rh was described by means of a relativistically adjusted effective core potential SDD for the inner electrons and its associated double-ζ basis set for the outer ones,[34] complemented with a set of f-polarization functions.[35] The 6-31G** basis set was used on H,[36] C, N, O, F, P, and Cl atoms,[37] including diffuse functions on O, F, and Cl atoms,[38] denoted 6-31(+)G**. In selected cases, the chloroform solvent has been described as a continuum (ε = 4.71) using the SMD method.[39] Geometries were optimized without any symmetry restrictions and the nature of the minima has been verified with analytical frequency calculations. Enthalpies have been computed at 298.15 K within the harmonic approximation.

Magnetic shielding tensors have been computed with the GIAO (gauge-including atomic orbitals) method[40] by means of the B3LYP functional[41] in gas phase as implemented in Gaussian 09. The basis set consisted in a well-tempered [16s10p9d] all-electron basis on Rh,[42] IGLO-basis DZ on H, and IGLO-basis II on the rest of atoms (denoted basis II').[43] Because functional and basis-set requirements are different for computing structural and spectroscopic parameters, such a mixed, "single-point" approach is common. This particular combination of levels has performed well in previous computations of ^{103}Rh chemical shifts.[16,18–22,44] In order to obtain the corresponding chemical shifts from the magnetic shieldings, a reference is needed. Due to the lack of a suitable compound, σ(standard) has been evaluated as the intercepts at δ = 0 of the σ(calc) vs. δ(expt) linear regressions involving complexes **1**–**7** (Figure 1) together with

several species which cover a wide range of the ^{103}Rh chemical shift window (see Figure S1 in Supporting Information).[16] The resulting σ(standard) values are −900 and −685 ppm for M06 and PBE0 geometries in gas phase, respectively. Then, the theoretical relative shifts have been calculated as follows, δ(calc) = σ(standard) − σ(calc).

Table 1. Selected geometrical parameters of **1**–**7** from theory (M06 or PBE0 optimized) and experiment (X-ray crystallography).

Compound	Method	Rh–P / Å		Rh–C(sp^2) / Å				P–Rh–P / °
	M06	2.317	2.318	2.236	2.276	2.238	2.276	82.7
1	PBE0	2.313	2.312	2.203	2.241	2.205	2.243	83.3
	X-ray[45]	2.291	2.267	2.239	2.250	2.235	2.238	83.2
	M06	2.319	2.318	2.223	2.272	2.223	2.272	83.0
2	PBE0	2.313	2.312	2.191	2.243	2.191	2.242	83.5
	X-ray[46]	2.276	2.259	2.211	2.273	2.209	2.267	83.3
	M06	2.311	2.311	2.225	2.285	2.224	2.284	84.4
3	PBE0	2.308	2.305	2.191	2.253	2.189	2.251	84.7
	X-ray[45]	2.278	2.268	2.215	2.258	2.207	2.238	84.7
	M06	2.374	2.367	2.216	2.273	2.232	2.264	92.0
4	PBE0	2.360	2.363	2.188	2.244	2.194	2.232	92.1
	X-ray[47]	2.318	2.343	2.220	2.221	2.266	2.254	90.7
	M06	2.367	2.391	2.209	2.268	2.236	2.265	92.6
5	PBE0	2.356	2.377	2.182	2.240	2.200	2.234	93.4
	X-ray[27]	2.325	2.329	2.204	2.259	2.241	2.248	92.4
	M06	2.385	2.385	2.238	2.264	2.240	2.265	89.7
6	PBE0	2.369	2.368	2.212	2.226	2.212	2.228	90.0
	X-ray[48]	2.304	2.329	2.282	2.195	2.236	2.232	88.7
7	M06	2.386	2.386	2.237	2.262	2.238	2.263	89.9
	PBE0	2.370	2.368	2.209	2.225	2.210	2.226	90.3

Results and Discussion

Computation of Geometries and ^{103}Rh Chemical Shifts

The cationic complexes reported by Fabrello et al.[27] (Figure 1) were optimized at two DFT levels in the gas phase. The geometry is a key issue in the computation of NMR properties, thus two widely employed functionals have been tested, namely M06 and PBE0 (see Computational Details).[49] Selected geometrical parameters of the computed structures are collected in Table 1

together with data extracted from X-ray studies. In general terms, the computed structures are in line with the experimental ones.[50] As commonly found using these or related DFT levels,[33] the theoretical Rh-ligand bond lengths tend to be overestimated. The optimized Rh–P bond distances in particular are enlarged in all complexes, by up to ca. 0.081 Å and 0.065 Å with M06 and PBE0, respectively (compound **6** in Table 1).

Table 2. B3LYP-computed ^{103}Rh chemical shifts using M06 and PBE0 gas-phase geometries of **1**–**7**.

Compound	δ(calc)[a]		δ(expt)[27]
	M06	PBE0	
1	−526	−431	−513
2	−518	−410	−503
3	−458	−347	−460
4	−147	−117	−278
5	−108	−88	−257
6	−42	−53	−98
7	−33	−45	−90
Slope[b]	1.22	0.92	
MAD[c]	60	101	

[a] Relative to the intercepts at δ = 0 of the σ(calc) vs. δ(expt) linear regressions (see Computational Details). [b] Slope of the δ(calc) vs. δ(expt) linear regression involving complexes **1**–**7**. [c] Mean absolute deviation from experiments.

Magnetic shieldings have been evaluated on the above-mentioned structures and the corresponding chemical shifts are collected in Table 2. The slopes of the δ(calc) vs. δ(expt) linear regressions are an indication how well the computed data follow the experimental trend (unity means ideal correlation). In this regard, with a slope of 1.22, M06 geometries afford a significant overestimation of the substituent effects on δ(^{103}Rh) (see the plot in Figure 2a), whereas PBE0 structures reproduce the trend much better, with a slope of 0.92 (Figure 2b). The good performance of PBE0 is in line with the better description of bond distances mentioned before. Nevertheless, the mean absolute deviation (MAD) between the calculated and the experimental chemical shifts is higher for the PBE0 than for the M06 geometries (last row in Table 2). From Figure 2 it is apparent that the seemingly small MAD for M06 arises from the fact that the computed and observed δ values happen to be very close to each other for complexes **1**–**3**, whereas the chemical shifts for the PBE0 structures are rather systematically overestimated. In the latter case, the shielding constant derived for the standard is dominated by the test set of carbonyl and cyclopentadienyl complexes far outside the shift range considered here (see Computational Details and Figure S1). The MAD for the PBE data of **1**–**7** could be reduced by fitting σ(standard) just for this subset, or by using one of these complexes as primary (internal) reference for the others. Neither option was attempted, however, in order to keep our protocol generally applicable. Finally, the NMR protocol was tested directly on non-optimized

single cations taken from the X-ray structures (after removing all co-crystallized species). Even though the global trend for complexes **1**–**4** and **6** is close to unity, the points are quite scattered (R^2 only 0.75, see Figure S2 in Supporting Information), and the results seem less trustworthy.

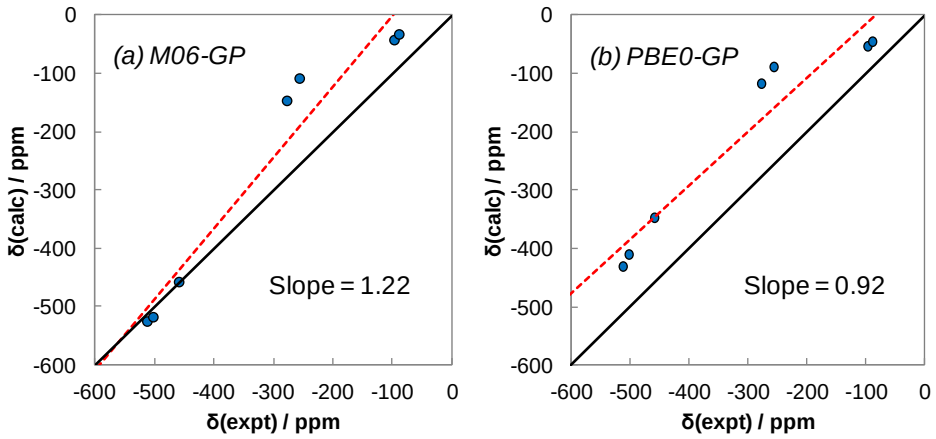

Figure 2. Plots of δ(^{103}Rh,calc) vs. δ(expt) according to geometries of **1**–**7** computed at (a) M06 and (b) PBE0 level in gas phase (GP). Regression lines in dashed red and ideal lines in solid black.

As discussed above, M06- and PBE0-optimized structures show noticeable differences in their metal–ligand bond distances (see Table 1). The key role of distance parameters on chemical shifts has been already noted.[18] In a computational experiment, complexes **1**–**7** were re-optimized using M06, but keeping all Rh–P and Rh–C(sp^2) bond distances constrained to the PBE0 data. In all cases, the energy difference between the fully relaxed and the fixed structures was lower than 0.5 kcal mol^{-1}. Subsequently, magnetic shieldings were computed as usual. The resulting values mostly mimic the PBE0 ones and afford a quite similar slope for the δ(calc) vs. δ(expt) linear regression, i.e. 0.93 (see Figure S3 in Supporting Information). Therefore, it can be concluded that the functional employed in the optimizations affects the chemical shifts mainly through the proper description of the metal–ligand bond distances.

To stress this point, ^{103}Rh NMR chemical shifts were computed on distorted structures of **1**. Starting from the fully optimized PBE0 geometry, the Rh–P bond distances were set at different values around the equilibrium distance (2.313 Å, Table 1), keeping the P–Rh–P bite angle β fixed and optimizing all other parameters (Figure 3a). In the same vein, several bite angles were tested, keeping the Rh–P bond distances fixed to the equilibrium value (Figure 3b). This protocol allows us to distinguish contributions from each of these geometrical parameters. In the first instance, the plot of δ(calc) vs. d(Rh–P) fits a line with a slope of 3184 ppm Å^{-1} (Figure 3a). This large value is in a range typical for many organometallic complexes of the middle and late transition rows.[51] Because of this high sensitivity of the metal chemical shift toward bond lengths, small errors in the latter can dramatically influence the former. On the other hand, much less influence can be perceived for the bite angle variation (Figure 3b). Though this set of data fits a polynomial function rather than a linear one, the effect of β can be estimated using a mean

Δδ/Δβ ratio of ca. 12 ppm degree^{-1} (maximum ca. 20 ppm degree^{-1} at 89 degrees). Overall, Rh–P bond distances emerge as the decisive parameters governing the ^{103}Rh chemical shifts of cationic bis(phosphine) complexes, in complete accord with previous findings for neutral acetylacetonato complexes,[18] or the Rh–N bonds in complexes with N-donor ligands.[20] The importance of the Rh–P bonds can be ascribed to inductive and resonance aspects together with polarization effects.[52]

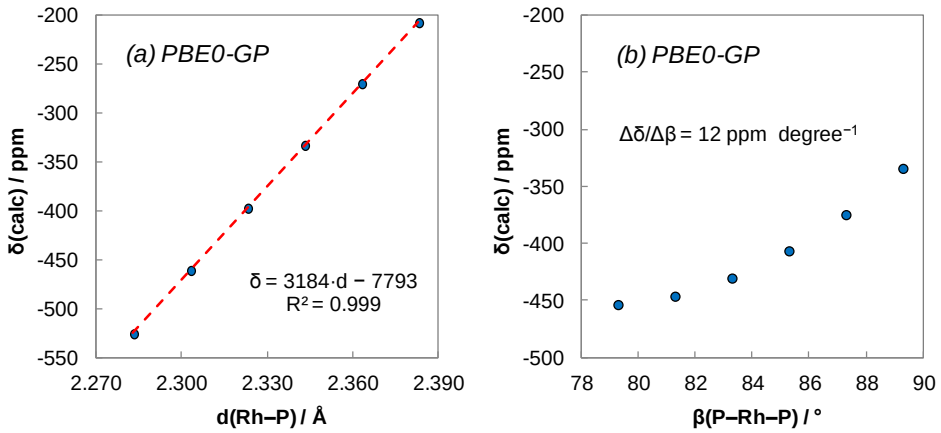

Figure 3. Variation of computed ^{103}Rh chemical shifts according to (a) Rh–P bond lengths and (b) P–Rh–P angles for PBE0-distorted geometries of **1**.

So far all computations have been performed in the gas phase. To probe how the environment in solution could affect the chemical shift, we decided to include the chloroform solvent used experimentally[27] as a continuum during optimization. The Rh–bis(phosphine) complexes were re-optimized under solvent conditions (**1s**–**7s**, where the "s" denotes optimized in solvent) and magnetic shieldings were computed in gas phase. Only minor changes in the Rh–P distances are found upon reoptimization (up to 0.007 Å). The slopes from the resulting δ(calc)[53] vs. δ(expt) plots are 1.20 and 0.93 for M06 and PBE0 geometries, respectively (mean absolute deviation of 67 and 119 ppm, respectively). In addition, the absolute slopes of the σ(calc) vs. δ(expt) plots using the SMD model solvent during the magnetic shielding computation are 1.22 and 0.95 for M06 and PBE0 geometries, respectively. Overall, they resemble the previous ones obtained in gas-phase conditions, i.e. 1.22 and 0.92 (see Table 2), and thus the inclusion of chloroform is not crucial in this scenario.

At first sight, counteranion effects are expected to be negligible as well, since experiments show similar chemical shifts when either $[PF_6]^-$, $[BF_4]^-$ or tosylate are present.[27] Nevertheless, pulsed gradient spin-echo (PGSE) diffusion studies for a cation related to **6** together with a variety of anions suggest appreciable extent of ion pairing in solution and different positional preferences for the anions, even though the ^{103}Rh chemical shifts are hardly affected (within less than 1 ppm).[54] Considering that the mere occurrence of ion pairing might affect the computational prediction, we have included an explicit $[PF_6]^-$ as prototypical counterion. Ion pairs **1s**·$[PF_6]$–**7s**·$[PF_6]$ were optimized under solvent conditions and magnetic shieldings were computed in gas phase. The counteranion was initially located at the apical position of the square-planar

complex. Upon optimization, PBE0 geometries show no remarkable contacts since the counteranions are located far away from the metal centers (with the shortest Rh···F distances well above 4 Å).[55] In contrast, M06 optimizations afford much tighter interactions, with Rh···F distances of ca. 3.5 Å. To illustrate this result, Figure 4 displays the disposition of the anion in **5s**·[PF_6]. Rh···F distances of **1s**·[PF_6]–**7s**·[PF_6] can be consulted at Table S1 in Supporting Information. It thus appears that in these complexes, ion paring is driven not only by Coulomb attraction, but also by dispersion.

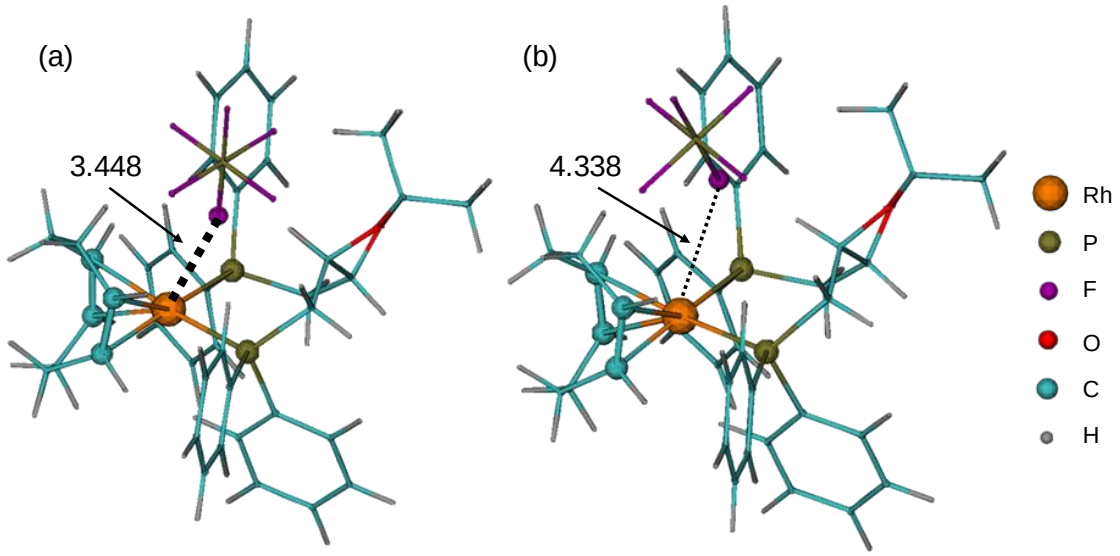

Figure 4. (a) M06- and (b) PBE0-optimized geometries of **5s**·[PF_6] (SMD solvent model). Distances in Å.

When the ^{103}Rh chemical shifts are evaluated for these ion pairs it appears that the complexes at the shielded end (**1s**·[PF_6]–**3s**·[PF_6]) are affected more strongly by the presence of the anion than those at the deshielded end. As a consequence, the slopes of the δ(calc)[53] vs. δ(expt) linear regressions decrease upon ion pairing from 1.22 and 0.92 (Figure 2) to 1.00 and 0.86 for M06 and PBE0 geometries, respectively (dashed red lines in Figure 5). In the latter case, the mean absolute deviations are now rather similar for M06 and PBE0 structures, 100 and 115 ppm, respectively. Both the physical presence of the anion and the distortion upon optimization may be responsible of these results. To distinguish them, the chemical shifts have been computed on **1s**·[PF_6]–**7s**·[PF_6] by removing the [PF_6]$^-$ moieties without further optimization (namely **1s'**–**7s'**, the prime denoting the "distorted" structures). The slopes coming from these anion-distorted geometries are 1.08 and 0.89 for M06 and PBE0, respectively (dashed grey lines in Figure 5). It can be deduced that the distortion of geometries rules the PBE0 approach whereas the M06 results are also governed by the physical presence of [PF_6]$^-$. The influence of the counteranion is thus more noticeable in the M06 calculations, probably due to the proper description of dispersion interactions.

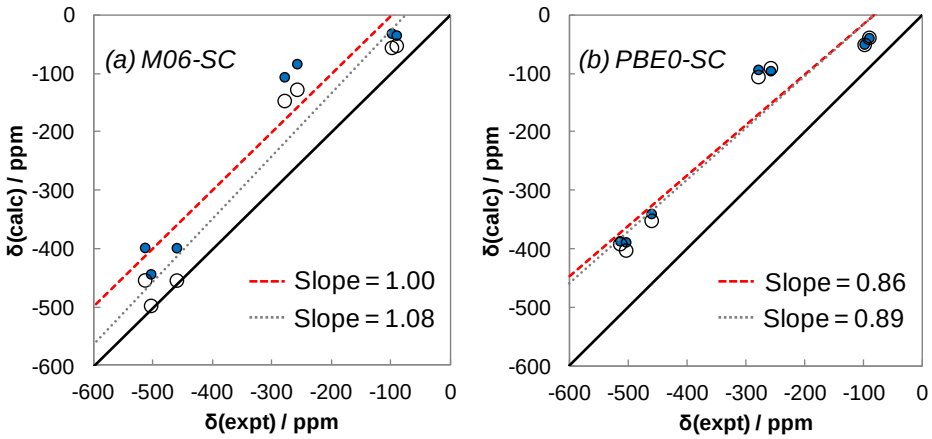

Figure 5. Plots of δ(^{103}Rh,calc) vs. δ(expt) for distorted (empty circles) and fully optimized (blue circles) geometries of **1s**·[PF_6]–**7s**·[PF_6] computed at (a) M06 and (b) PBE0 level in chloroform solvent (SMD model). Regression lines in dashed red and grey and ideal lines in solid black.

To sum up this section, Rh–P bond distances are revealed as key parameters in the computation of ^{103}Rh chemical shifts of Rh–bis(phosphine) complexes. The PBE0 functional provides suitable gas-phase geometries for routine calculations and is, thus, the simplest approach which provides reasonably accurate results for chemical shift trends. However, when the counteranion is explicitly considered, dispersion interactions should be taken into account during optimization (e.g. via the M06 functional).

Systematic Analysis of ^{103}Rh Chemical Shifts

We will now use our "simple" theoretical protocol, i.e. B3LYP magnetic shieldings on gas-phase PBE0 geometries without counterions, to study in more detail how the ^{103}Rh chemical shifts depend on the chemical environment. To achieve this goal, a new set of cationic complexes was generated by systematically changing the bis(phosphine) ligand in **1** through modifying the chelating ring size (n = 2, 3, 4) and the groups attached to the phosphorous atoms (R = H, CH_3, CF_3, Ph, and Cy, affording complexes **8**–**20**, Figure 6). No exhaustive confomational searches were undertaken for these flexible ring systems; for the five- and seven-membered rings, conformations were taken from the previous gas-phase optimizations of **1** and **4**, respectively, for the six-membered rings (n = 3), a chair-like conformation was adopted as found in a reported solid-state structure.[56]

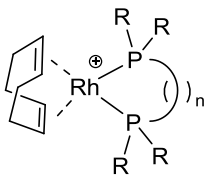

R = H n = 2 (**8**), 3 (**9**), 4 (**10**)
CH_3 n = 2 (**11**), 3 (**12**), 4 (**13**)
CF_3 n = 2 (**14**), 3 (**15**), 4 (**16**)
Ph n = 2 (**1**), 3 (**17**), 4 (**4**)
Cy n = 2 (**18**), 3 (**19**), 4 (**20**)

Figure 6. Substitution pattern of complexes derived from **1**.

A key property to which the ^{103}Rh shifts may be correlated (in the spirit of reference 21) is the relative stability of the complexes. To probe the donor properties of the various bis(phosphine) ligands, ligand exchange is assessed through the isodesmic reactions in Scheme 1. The free ligands were optimized in all-s-*trans* conformations[57] free of clashes between PR_2 groups. We will discuss relative enthalpies in gas phase, ΔH_{iso} (PBE0 SDD/6-31G**), which are referred to **11** (more negative ΔH_{iso} values denoting higher affinity of the ligand to coordinate to rhodium).

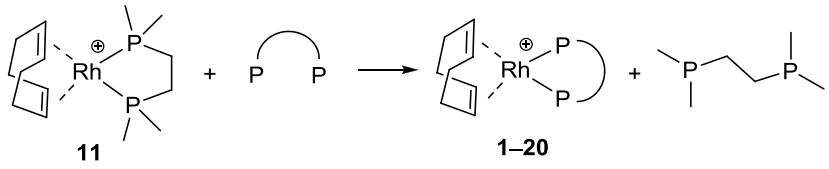

Scheme 1. Isodesmic ligand exchange reactions (**11** taken as reference).

δ(calc) vs. ΔH_{iso} values of species **1**–**7** are plotted in Figure 7a. In agreement with previous Gibbs energy results,[27] complexes **1**–**3** are characterized by strongly binding bis(phosphine) ligands (i.e. good donors) and rather shielded ^{103}Rh nuclei, whereas complexes **4**–**7** show higher ΔH_{iso} values and more deshielded δ(^{103}Rh). It thus appears as if ΔH_{iso} values could be related with chemical shifts, at least qualitatively. However, this trend cannot be generalized to all kind of ligands, as apparent for the corresponding results for species **1**, **4**, and **8**–**20** as shown in Figure 7b. For sets of complexes bearing the same group R, the increment of the chelating size n increases both the chemical shift and ΔH_{iso} (excluding R = H for the latter). As expected for electron-poor ligands, species containing CF_3 groups show high positive ΔH_{iso} values (35–42 kcal mol^{-1}), followed by those with R = H (15–18 kcal mol^{-1}). Then, methyl (CH_3), phenyl (Ph) and cyclohexyl (Cy) derivatives exhibit similar enthalpies within the same chelating size. This general trend in ΔH_{iso} as a function of the electron-withdrawing or -donating capabilities of the ligand is not reflected in concomitant changes in δ(^{103}Rh), so that for the evaluated cases no overall correlation between chemical shifts and stabilities can be deduced. This result corroborates similar findings for Rh–bis(olefin) complexes, where an empirical chemical shift–stability correlation could be reproduced only for very closely related (alkyl-substituted) olefins, but was not predicted to extend to olefins with different electronic properties (e.g. fluorinated ones).[21]

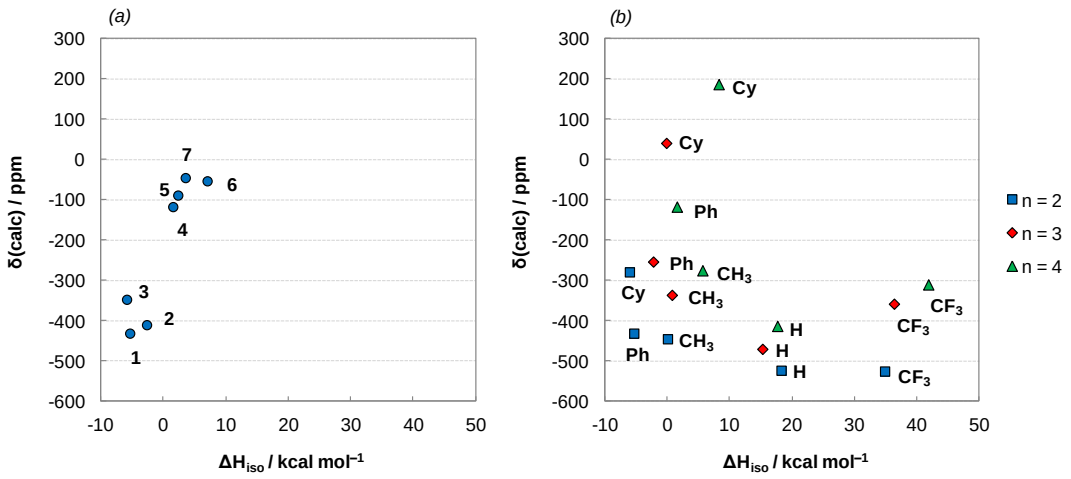

Figure 7. Plots of δ(^{103}Rh,calc) vs. ΔH_{iso} according to species (a) **1**–**7** and (b) **1**, **4** and **8**–**20**.

On the other hand, the average Rh–P bond distance appears as an excellent probe into the chemical shifts. Figure 8a shows the δ(calc) vs. d(Rh–P) plot regarding species **1**–**7**. A linear regression can be estimated with a slope of 5682 ppm Å^{-1} (R^2 = 0.952).[58] More importantly, essentially the same linear correlation holds also for complexes **1**, **4** and **8**–**20** (see Figure 8b). The individual slopes of complexes with n = 2, 3, and 4 are 3583 ppm Å^{-1} (R^2 = 0.867), 5862 ppm Å^{-1} (R^2 = 0.933), and 5513 ppm Å^{-1} (R^2 = 0.988), respectively. A good global correlation can be detected displaying a similar slope of 5285 ppm Å^{-1} (R^2 = 0.940),[59] although some deviations are found for the five-membered ring species (n = 2). Overall, ^{103}Rh chemical shifts emerge as sensitive indicators for Rh–P bond distances and may be useful tools to describe chemical shift–structure relationships including bis(phosphine) ligands with different chelating sizes and electron-donor groups. Because stronger bonds to transition metals are not always associated with shorter bond distances,[60] this correlation does not necessarily translate into chemical shift–stability relationships.

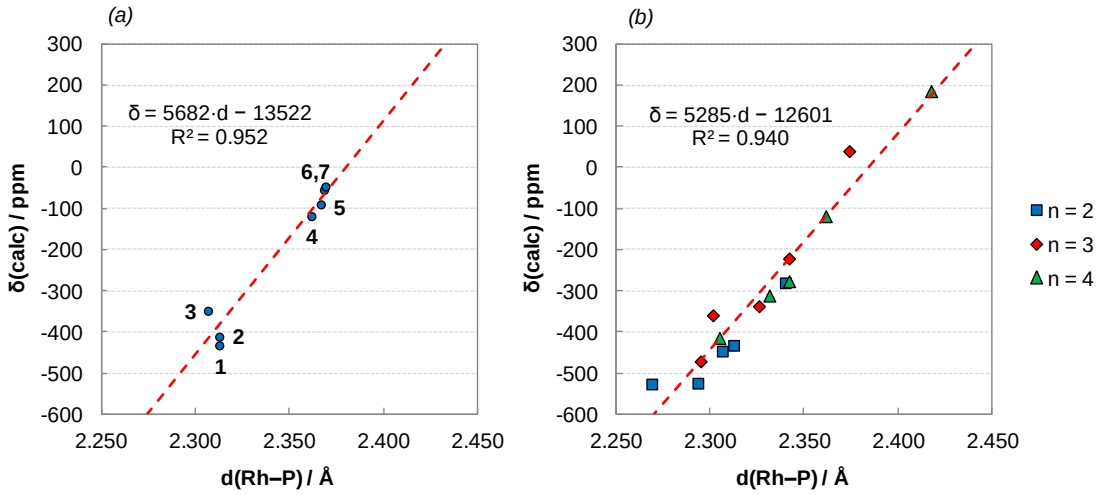

Figure 8. Plots of δ(^{103}Rh,calc) vs. average d(Rh–P) according to species (a) **1**–**7** and (b) **1**, **4** and **8**–**20**.

To probe the generality of this trend linking shifts and Rh–P distances, we analyzed even more subtle variations of the ligands. Inspired by the substituting pattern in complexes **6** and **7**, the substituents in *para* position of the aryl groups of **6** were varied by OH (**21**), F (**22**), Cl (**23**), and CF_3 (**24**). These groups (including H and CH_3) can be described using Hammett σ_p constants,[61] which are usually related to inductive effects. Figure 9a displays the δ(calc) vs. σ_p fitting function concerning **6**, **7** and **21**–**24**. Linear relationships between ^{103}Rh chemical shifts and Hammett constants have been reported previously.[5,18] In all cases, including our systems, the remote electron-withdrawing groups cause a shielding of the metal, in line with observations that an increase in phosphine basicity shifts the metal resonances to higher frequencies. Interestingly, even though the ^{103}Rh chemical shift span is narrow, ca. 40 ppm, the computed values still correlate with average Rh–P bond distances at the picometer scale (Figure 9b).[62]

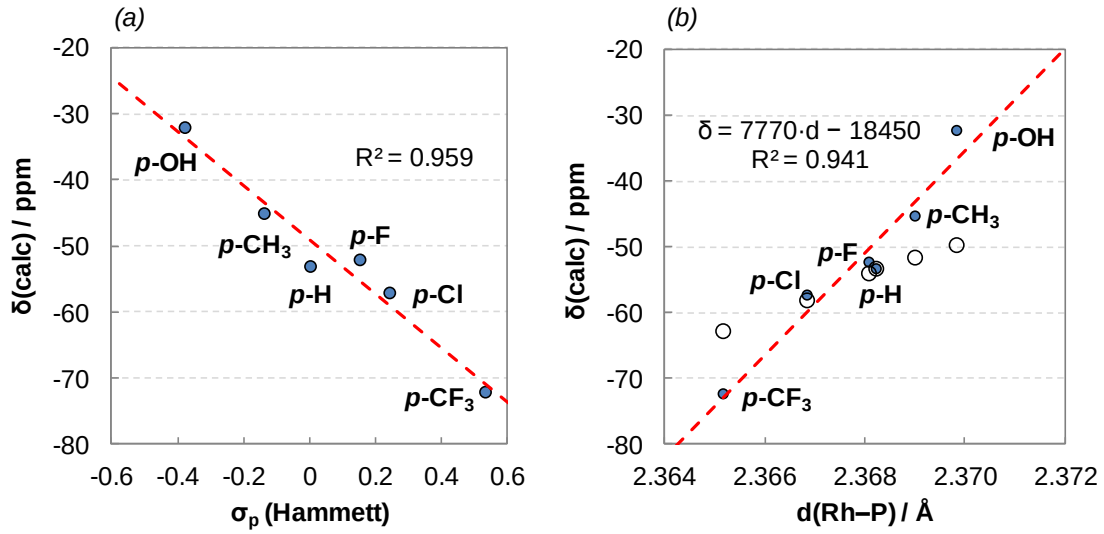

Figure 9. Plots of δ(^{103}Rh,calc) vs. (a) Hammett σ_p constants and (b) average d(Rh–P) according to species **6**, **7** and **21**–**24**. Open circles: results for partially optimized structures of **6** (*p*-H), see text.

The slope of the correlation in Figure 9b, ca. 7800 ppm Å^{-1}, is somewhat larger than that for the "regular" complexes (**1**–**20**) in Figure 8, where it amounts to ca. 5300–5700 ppm Å^{-1}. Nevertheless, the similarity of these slopes suggests that such remote "Hammett" substituents might affect δ(^{103}Rh) to a large extent indirectly, namely through tuning the Rh–P distances, rather than directly through a modified response of the electronic wavefunction to the magnetic field. The latter, electronic effect can be separated computationally by changing the *para*-substituent in **7** and **21**–**24** to H and keeping the same Rh–P distance (i.e. affording "distorted" versions of the parent **6**). If the NMR calculations are repeated without reoptimization, no clear trend is apparent. When the structures are relaxed with the Rh–P distance fixed, the open circles in Figure 9b are obtained. The slope of a linear fit is 2877 ppm Å^{-1} (R^2=0.994), similar to that obtained for **1** (ca. 3200 ppm Å^{-1}, Figure 3a). Even though steric and electronic effects are not fully disentangled this way, it appears that the indirect effect via the bond distance can be substantial, in particular for the electron-withdrawing substituents such as Cl or CF_3.[63] In summary, the inductive effects of remote substituents described by their Hammett constants affect the ^{103}Rh chemical shifts not only directly through the electronic structure, but also indirectly through their influence on the Rh–P bond distances.

Analogous modifications including OH, CH_3, F, Cl, and CF_3 groups in *para* position were implemented in **1** (**25**–**29**), **17** (**30**–**34**), and **4** (**35**–**39**). The corresponding linear regressions of chemical shift against both Hammett constant and Rh–P bond distance can be found in Figures S4–S6 in Supporting Information. The quality of these trends ranges from moderate (R^2 = 0.78 for the derivates of **1**) to good (R^2 = 0.91 for the derivates of **4**), with slopes between ca. 7500–10500 ppm Å^{-1}. Some scatter is detected when dealing with the five-membered rings (n = 2), whereas the set with n = 4 follows well the expected correlation (Figure 9). Therefore, to obtain

an overall picture some additional factors, such as the chelating size, should also be taken into account.

Conclusions

^{103}Rh NMR chemical shifts have been computed for a series of cationic Rh–bis(phosphine) complexes at the B3LYP level of DFT and have been critically compared to experiments. PBE0 geometries of isolated species in the gas phase provide good chemical shift trends suitable for routine calculations. When the counteranion is explicitly considered, dispersion-included methods such as M06 are recommended for geometry optimizations.

For a small subset of the studied compounds one can note common trends between $\delta(^{103}\text{Rh})$ values and complex stabilities (evaluated through isodesmic ligand exchange reaction energies). However, no clear correlation between these properties is apparent for the full set studied. Instead, a decrease of Rh–P bond lengths entails a shielding of the ^{103}Rh nuclei through a linear relationship, which holds remarkably well for a large variety of substituents at P and chelating ring sizes. This behavior has also been detected in more subtle variations of the electronic properties of the ligands, where it could be related to Hammett σ_p constants. The simultaneous combination of steric and electronic effects is inherently responsible for metal–ligand bond distances, which in turn are decisive for transition metal chemical shifts. The scope of these results is to shed light on future structure–reactivity correlations assisted by NMR techniques and to apply first-principles electronic-structure computations for enhancing the usefulness of transition metal NMR spectroscopy as a structural tool. The latter aspect could be expanded by further studies into the role of the spectator ligand(s), COD in our case, and how they influence the salient NMR–structure relationships.

Acknowledgments

MB and LC wish to thank EaStCHEM and the EPSRC for support. Computations were carried out on a local Opteron PC cluster maintained by Dr. H. Früchtl. MAO is also grateful to the Spanish MECD for a FPU research grant.

References

1 *Transition Metal Nuclear Magnetic Resonance*; Pregosin, P. S. Ed.; Elsevier: Amsterdam, 1991.

2 (a) von Philipsborn, W. *Chem. Soc. Rev.* **1999**, *28*, 95–105. (b) Ernsting, J. M.; Gaemers, S.; Elsevier, C. J. *Magn. Reson. Chem.* **2004**, *42*, 721–736. (c) Carlton, L. *Ann. R. NMR S.* **2008**, *63*, 49–178.

3 Damoense, L.; Datt, M.; Green, M.; Steenkamp, C. *Coord. Chem. Rev.* **2004**, *248*, 2393–2407.

4 Carlton, L. *J. Organomet. Chem.* **1992**, *431*, 103–115. (b) Elsevier, C. J.; Kowall, B.; Kragten, H. *Inorg. Chem.* **1995**, *34*, 4836–4829. (c) Börner, A.; Kless, A.; Holz, J.; Baumann, W.; Tillack, A.; Kadyrov, R. *J. Organomet. Chem.* **1995**, *490*, 213–219.

5 Bregman, F. R.; Ernsting, J. M.; Müller, F.; Boele, M. D. K.; van der Veen, L. A.; Elsevier, C. J. *J. Organomet. Chem.* **1999**, *592*, 306–311.

[6] Filipuzzi, S.; Männel, E.; Pregosin, P. S.; Albinati, A.; Rizzato, S.; Veiros, L. F. *Organometallics* **2008**, *27*, 4580–4588.

[7] Koller, M.; von Philipsborn, W. *Organometallics* **1992**, *11*, 467–469.

[8] Tedesco, V.; von Philipsborn, W. *Organometallics* **1995**, *14*, 3600–3602.

[9] Bender, B. R.; Koller, M.; Nanz, D.; von Philipsborn, W. *J. Am. Chem. Soc.* **1993**, *115*, 5889–5890.

[10] Åkermark, B.; Blomberg, M. R. A.; Glaser, J.; Öhrström, L.; Wahlberg, S.; Wärnmark, K.; Zetterber, K. *J. Am. Chem. Soc.* **1994**, *116*, 3405–3413.

[11] Houston, J. R.; Olmstead, M. M.; Casey, W. H. *Inorg. Chem.* **2006**, *45*, 7799–7805.

[12] Bönnemann, H.; Brijoux, W.; Brinkmann, R.; Meurers, W.; Mynott, R. *J. Organomet. Chem.* **1984**, *272*, 231–249.

[13] Bühl, M. *Angew. Chem. Int. Ed.* **1998**, *37*, 142–144.

[14] (a) Schreckenbach, G.; Ziegler, T. *Int. J. Quantum Chem.* **1997**, *61*, 899–918. (b) Schreckenbach, G.; Ziegler, T. *Theor. Chem. Acc.* **1998**, *99*, 71–82. (c) Bühl, M.; Kaupp, M.; Malkina, O. L.; Malkin, V. G. *J. Comput. Chem.* **1999**, *20*, 91–105. (d) Bühl, M. *Ann. R. NMR S.* **2008**, *64*, 77–126.

[15] (a) *Calculation of NMR and EPR Parameters. Theory and Applications*; Kaupp, M.; Bühl, M.; Malkin, V. G. Eds.; Wiley-VCH: Weinheim, 2004. (b) Kaupp, M.; Bühl, M. in: *Computational Inorganic and Bioinorganic Chemisty* (*Encyclopedia of Inorganic and Bioinorganic Chemistry*), R. B. King (Ed.), Wiley, New York, 2009, pp. 91–108.

[16] Bühl, M. *Chem. Phys. Lett.* **1997**, *267*, 251–257.

[17] Bühl, M. *Organometallics* **1997**, *16*, 261–267.

[18] Leitner, W.; Bühl, M.; Fornika, R.; Six, C.; Baumann, W.; Dinjus, E.; Kessler, M.; Krüger, C.; Rufińska, A. *Organometallics* **1999**, *18*, 1196–1206.

[19] Bühl, M.; Baumann, W.; Kadyrov, R.; Börner, A. *Helv. Chim. Acta* **1999**, *82*, 811–820.

[20] Donkervoort, J. G.; Bühl, M.; Ernsting, J. M.; Elsevier, C. J. *Eur. J. Inorg. Chem.* **1999**, 27–33.

[21] Bühl, M.; Håkansson, M.; Mahmoudkhani, A. H.; Öhrström, L. *Organometallics* **2000**, *19*, 5589–5596.

[22] Ramalho, T. C.; Bühl, M.; Figueroa-Villar, J. D.; de Alencastro, R. B. *Helv. Chim. Acta* **2005**, *88*, 2705–2721.

[23] Orian, L.; Bisello, A.; Santi, S.; Ceccon, A.; Saielli, G. *Chem. Eur. J.* **2004**, *10*, 4029–4040.

[24] Munro, O. Q.; Camp, G. L.; Carlton, L. *Eur. J. Inorg. Chem.* **2009**, 2512–2523.

[25] *The Handbook of Homogeneous Hydrogenation*; de Vries, J. G.; Elsevier, C. J. Eds.; Vol. 1–3, Wiley-VCH: Weinheim, 2007.

[26] Fabrello, A.; Bachelier, A.; Urrutigoïty, M.; Kalck, P. *Coord. Chem. Rev.* **2010**, *254*, 273–287.

[27] Fabrello, A.; Dioni, C.; Perrin, L.; Kalck, P.; Maron, L.; Urrutigoïty, M.; Dechy-Cabaret, O. *Magn. Reson. Chem.* **2010**, *48*, 848–856.

[28] Zhao, Y.; Truhlar, D. G. *Theor. Chem. Acc.* **2008**, *120*, 215–241.

[29] Wheeler, S. E.; Houk, K. N. *J. Chem. Theory Comput.* **2010**, *6*, 395–404.

[30] (a) Perdew, J. P.; Burke, K.; Ernzerhof, M. *Phys. Rev. Lett.* **1996**, *77*, 3865–3868. (b) Perdew, J. P.; Ernzerhof, M.; Burke, K. *J. Chem. Phys.* **1996**, *105*, 9982–9985.

[31] Gaussian 09, Revision A.02, Frisch, M. J. et al.

[32] (a) Zhao, Y.; Truhlar, D. G. *Acc. Chem. Res.* **2008**, *41*, 157–167. (b) Zhao, Y.; Truhlar, D. G. *Chem. Phys. Lett*. **2011**, *502*, 1–13.

[33] Waller, M. P.; Braun, H.; Hojdis, N.; Bühl, M. *J. Chem. Theory Comput.* **2007**, *3*, 2234–2242.

[34] Andrae, D.; Häußermann, U.; Dolg, M.; Stoll, H.; Preuß, H. *Theor. Chim. Acta* **1990**, *77*, 123–141.

[35] Ehlers, A. W.; Böhme, M.; Dapprich, S.; Gobbi, A.; Höllwarth, A.; Jonas, V.; Köhler, K. F.; Stegmann, R.; Veldkamp, A.; Frenking, G. *Chem. Phys. Lett.* **1993**, *208*, 111–114.

[36] Hehre, W. J.; Ditchfield, R.; Pople, J. A. *J. Chem. Phys.* **1972**, *56*, 2257–2261.

[37] Francl, M. M.; Pietro, W. J.; Hehre, W. J.; Binkley, J. S.; Gordon, M. S.; DeFrees, D. J.; Pople, J. A. *J. Chem. Phys.* **1982**, *77*, 3654–3665.

[38] Clark, T.; Chandrasekhar, J.; Spitznagel, G. W.; Schleyer, P. V. R. *J. Comput. Chem.* **1983**, 4, 294–301.

[39] Marenich, A. V.; Cramer, C. J.; Truhlar, D. G. *J. Phys. Chem. B* **2009**, *113*, 6378–6396.

[40] Cheeseman, J. R.; Trucks, G. W.; Keith, T. A.; Frisch, M. J. *J. Chem. Phys.* **1996**, *104*, 5497–5509.

[41] (a) Becke, A. D. *J. Chem. Phys.* **1993**, *98*, 5648–5652. (b) Lee, C.; Yang, W.; Parr, R. G. *Phys. Rev. B* **1988**, *37*, 785–789.

[42] Huzinaga, S.; Klobukowski, M. *J. Mol. Struct.* **1988**, *167*, 1–209.

[43] IGLO stands for Individual Gauge for Localized Orbitals, a Coupled Hartree-Fock variant, for which these basis sets were originally developed: Kutzelnigg, W.; Fleischer, U.; Schindler, M. in *NMR Basic Principles and Progress* Vol. 23; Springer Verlag, Berlin, 1990; p 165.

[44] In contrast to the geometry optimizations and energy/enthalpy calculations (which include scalar relativistic effects), magnetic shieldings are computed at a non-relativistic level. While relativity can affect these absolute shieldings significantly, this effect tends to be very systematic for 3d- and 4d-metal nuclei, so that (in the absence of strong spin-orbit coupling) the relativistic effects cancel to a large extent in the relative chemical shifts, see e.g. reference 14d.

[45] Drexler, H.-J.; Zhang, S.; Sun, A.; Spannenberg, A.; Arrieta, A.; Preetz, A.; Heller, D. *Tetrahedron: Asymm.* **2004**, *15*, 2139–2150. CSD entries IBOZIJ and IBUBAJ.

[46] Burk, M. J.; Feaster, J. E.; Harlow, R. L. *Organometallics* **1990**, *9*, 2653–2655. CSD entry JEWZOA.

[47] Anderson, M. P.; Pignolet, L. H. *Inorg. Chem.* **1981**, *20*, 4101–4107. CSD entry BEDPIJ.

[48] Preetz, A.; Drexler, H.-J.; Schulz, S.; Heller, D. *Tetrahedron: Asymm.* **2010**, *21*, 1226–1231. CSD entry SUXFUR.

[49] The BP86 functional, employed for most of the previous optimizations of small and medium-sized Rh complexes (see references 16–22), is expected to be less accurate for the present set of bulky ligands, because the lack of dispersion in this functional is expected to produce overly long Rh–ligand bond distances. While such overestimated distances may still be acceptable to compute refined energies (see e.g. Sieffert, N.; Bühl, M. *Inorg. Chem*. **2009**, *48*, 4622–4624), they may be detrimental for the Rh chemical shifts.

[50] The calculated geometries for **1**, **3** and **4** are not exactly the same as the X-ray structure due to the conformation of the COD ligand (involving $C(sp^2)$–$C(sp^3)$–$C(sp^3)$–$C(sp^2)$ dihedral angles), but they are more stable in the gas phase.

[51] Grigoleit, S.; Bühl, M. *Chem. Eur. J.* **2004**, *10*, 5541–5552.

[52] (a) Egorochkin, A. N.; Kuznetsova, O. V.; Khamaletdinova, N. M.; Kurskii, Y. A.; Domratcheva-Lvova, L. G.; Domrachev, G. A. *Magn. Reson. Chem.* **2009**, *47*, 782–790. (b) Egorochkin, A. N.; Kuznetsova, O. V.; Khamaletdinova, N. M.; Kurskii, Y. A. *Russ. J. Gen. Chem.* **2011**, *81*, 2450–2458.

[53] σ(standard) obtained from gas-phase geometries, see Computational Details.

[54] Kumar, P. G. A.; Pregosin, P. S.; Schmid, T. M.; Consiglio, G. *Magn. Reson. Chem.* **2004**, *42*, 795–800.

[55] Even in a continuum, charged molecules are unlikely to separate spontaneously. However, with distances this large, we can consider that no strong direct interaction involving the metal is present.

[56] Kempe, R.; Spannenberg, A.; Heller, D. *Z. Kristallogr.-New Cryst. Struct.* **2001**, *216*, 153–156. CSD entry QOPJUA.

[57] For the free ligands of **19** and **20**, P–C–C–P dihedral angles of ca. 60° provided structures with lower enthalpies.

[58] δ(^{103}Rh) of the "real" systems thus appears to be slightly more sensitive to the Rh–P distance as compared to the analysis from the constrained optimizations in complex **1**, where this slope amounted to ca. 3200 ppm Å^{-1} (see Figure 3a).

[59] The slope concerning species **1**–**20** is 5338 ppm Å^{-1} (R^2 = 0.943).

[60] See e.g.: (a) Ernst, R. D.; Freeman, J. W.; Stahl, L.; Wilson, D. R.; Arif, A. M.; Nuber, B.; Ziegler, M. L. *J. Am. Chem. Soc.* **1995**, *117*, 5075–5081. (b) Frenking, G.; Wichmann, K.; Fröhlich, N.; Grobe, J.; Golla, W.; Le Van, D.; Krebs, B.; Lage, M. *Organometallics* **2002**, *21*, 2921–2930.

[61] March, J. *Advanced Organic Chemistry*, 3rd ed.; Wiley, New York, 1985, p 244.

[62] Even more subtle structural variations can be resolved using ^{103}Rh NMR, namely $^{35/37}$Cl isotope effects in Rh(III) chloro aquo complexes, where the changes in Rh–Cl bonds between the isotopomers are on the femtometer scale, see e.g.: Davis, J. C.; Bühl, M.; Koch, K. R. *J. Phys. Chem. A* **2013**, *117*, 8054−8064..

[63] The correlations in Figure 8 may also contain such "direct" electronic (inductive) effects from the various substituents, but except for the CF_3 derivatives **14**–**16** these effects should be rather similar, so that the Rh–P distance is indeed the decisive parameter.

TOC graphic

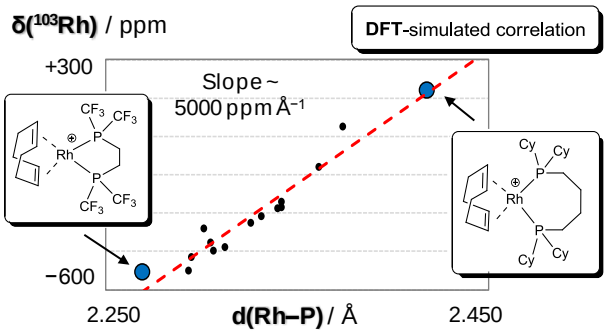
δ(103Rh) / ppm
DFT-simulated correlation
+300
Slope ~
5000 ppm Å-1
−600
2.250
d(Rh–P) / Å
2.450
CF3
CF3
P
Rh
P
CF3
CF3
Cy
Cy
P
Rh
P
Cy
Cy